

# Rational Approximations for Oscillatory Two-Parameter Mittag-Leffler Function

Aljowhara H. Honain<sup>a,b</sup>, Khaled M. Furati<sup>a,c</sup>, Ibrahim O. Sarumi<sup>a,d</sup>, Abdul Q. M. Khaliq<sup>e</sup>

<sup>a</sup>*King Fahd University of Petroleum & Minerals  
Department of Mathematics  
Dhahran, Saudi Arabia*

<sup>b</sup>*g201907570@kfupm.edu.sa*

<sup>c</sup>*kmfurati@kfupm.edu.sa*

<sup>d</sup>*ibrahim.sarumi@kfupm.edu.sa*

<sup>e</sup>*Middle Tennessee State University  
Department of Mathematical Sciences  
Murfreesboro, TN, USA  
abdul.khaliq@mtsu.edu*

---

## Abstract

The two-parameter Mittag-Leffler function  $E_{\alpha,\beta}$  is of fundamental importance in fractional calculus. It appears frequently in the solutions of fractional differential and integral equations. Nonetheless, this vital function is often expensive to compute. Several attempts have been made to construct cost-effective and accurate approximations. These attempts focus mainly on the completely monotone Mittag-Leffler functions. However, when  $\alpha > 1$  the monotonicity property is largely lost and as such roots and oscillations are exhibited. Consequently, existing approximants constructed mainly for  $\alpha \in (0, 1)$  often fail to capture this oscillatory behavior. In this paper, we construct computationally efficient and accurate rational approximants for  $E_{\alpha,\beta}(-t)$ ,  $t \geq 0$ , with  $\alpha \in (1, 2)$ . This construction is fundamentally based on the decomposition of Mittag-Leffler function with real roots into one without and a polynomial. Following which new approximants are constructed by combining the global Padé approximation with a polynomial of appropriate degree. The rational approximants are extended to approximation of matrix Mittag-Leffler and different approaches to achieve efficient implementation for matrix arguments are discussed. Numerical experiments are provided to illustrate the significant accuracy improvement achieved by the proposed approximants.

**Keywords:** Oscillatory Mittag-Leffler function; Global Padé approximation; Fractional oscillation equations; Fractional plasma oscillations; Fractional diffusion-wave equation

---

## 1. Introduction

We are concerned with the approximation of the two parameter Mittag-Leffler function (MLF)  $E_{\alpha,\beta}$ , defined by

$$E_{\alpha,\beta}(z) = \sum_{k=0}^{\infty} \frac{z^k}{\Gamma(\alpha k + \beta)}, \quad \operatorname{Re} \alpha > 0, \beta \in \mathbb{C}, \quad z \in \mathbb{C}. \quad (1)$$

This entire function generalizes the MLF of one-parameter,  $E_{\alpha} = E_{\alpha,1}$ , and contains several well-known special functions as special cases. In particular,  $E_1$  is the exponential function,  $E_2(-z^2)$  and  $zE_{2,2}(-z^2)$  are the cosine and sine functions, respectively, among others. For some surveys on the Mittag-Leffler functions, see for example [1, 2].

The Mittag-Leffler function  $E_{\alpha,\beta}(z)$  arises frequently in the solutions of many physical problems described by differential and/or integral equations of fractional order. In the case  $\alpha \in (1, 2)$ , the MLF appears naturally in the solutions of fractional diffusion-wave equations, fractional differential equation for motion, and fractional plasma equations, see [3, 4, 5, 6, 7].

Computing the MLF  $E_{\alpha,\beta}$  is usually challenging (devising and implementing suitable algorithms) and expensive (computation time). Although the series (1) converges for all  $z \in \mathbb{C}$ , it is impractical or ineffective to use it computationally for  $|z| \geq 1$  because the series converges very slowly. As a result, various methods have been developed to evaluate the MLF. In [8], an algorithm based on the location of the argument  $z$  in the complex plane is developed, whereby for large  $|z|$  values the asymptotic series as  $|z| \rightarrow \infty$  is used, for  $|z| < 1$  the series definition (1) is used, and for values in intermediate regions the integral representation is used. In [9], an approach based on numerical inversion of Laplace transform is proposed. However, these approaches are often computationally time consuming, see [10, 11] for some CPU-time comparisons.

Various rational approximations have been sought to approximate  $E_{\alpha,\beta}$  efficiently and accurately. Some of them are based solely on the series definition and provide accurate approximations for small argument values, see for example [12, 13, 14]. Some others are based on global Padé approach [15] in which a hybrid of the local series definition and the asymptotic series representation is used. These global approximations lead to approximants that are accurate over a wide range of arguments, see [16, 17, 18, 10, 11].

The existing rational approximants are effective when the MLF is completely monotone, which is the case when  $\alpha \in (0, 1)$  and  $\beta \geq \alpha$ . However, when  $\alpha > 1$ , as discussed in [19, 20, 21], for some  $\alpha$ - $\beta$  combinations,  $E_{\alpha,\beta}$  is often oscillatory and having multiple real zeros. In these situations, the rational approximants might fail to trace the oscillation profile and match the large zeros.

In this paper, we consider in the  $\alpha\beta$ -plane the strip

$$\Omega = \{(\alpha, \beta) : 1 < \alpha < 2, \beta \geq 1\}. \quad (2)$$

The regions where  $E_{\alpha,\beta}$  is monotone and where it is oscillatory are classified by studying the zeros of its derivative. In addition, we introduce new rational approximants that sufficiently capture more of the MLF roots and are able to trace their oscillations. This is achieved by decomposing  $E_{\alpha,\beta}$  into one without and a polynomial. Based on this decomposition, we construct new rational approximants as a sum of the global Padé approximant and a polynomial. Using this approach, we are able to capture sufficiently many roots of  $E_{\alpha,\beta}$  by choosing the appropriate degree of the polynomial. Further, we generalize these approximants to matrix MLF and discuss different approaches in which the approximant can be implemented for matrix arguments. Apart from the computation cost, all approaches yield close approximations.

Numerical experiments are presented to illustrate the performance of our approximants. Considering MLF with scalar arguments, we observe the limitation of the existing global Padé approximants in approximating the oscillatory MLFs. It is then demonstrated that the new approximants introduced here are able to improve the situation thereby providing sufficiently accurate approximations. For the matrix MLF, we consider four approaches for computing the rational approximants and compare them to the matrix MLF algorithm developed in [22]. Using the values obtained from this algorithm as a reference, it is seen that our approximants provide close values with significantly less computation time.

The rest of the paper is organized as follows: a characterization of the oscillatory behavior of the MLF is given in Section 2. In Section 3, the derooting representation is discussed. Global Padé approximants of MLF with scalar and matrix arguments are discussed in sections 4 and 5, respectively. Some applications to the evaluation of solutions of fractional evolution equations are discussed in Section 6.

## 2. Monotonicity and oscillatory properties

In this section, we characterize the oscillatory behavior of

$$E_{\alpha,\beta}(-t), \quad (\alpha, \beta) \in \Omega, \quad t \geq 0.$$

For the discussion that follows, the following formula for the derivative [1] plays a fundamental role:

$$\frac{d}{dt}E_{\alpha,\beta}(-t) = -\frac{1}{\alpha} [E_{\alpha,\beta+\alpha-1}(-t) - (\beta-1)E_{\alpha,\beta+\alpha}(-t)]. \quad (3)$$

Since  $E_{\alpha,\beta}(0) = 1/\Gamma(\beta)$ , it follow from (3) that

$$\frac{d}{dt}E_{\alpha,\beta}(0) = -\frac{1}{\alpha} \left[ \frac{1}{\Gamma(\beta+\alpha-1)} - \frac{\beta-1}{\Gamma(\beta+\alpha)} \right] = -\frac{1}{\Gamma(\beta+\alpha)} < 0. \quad (4)$$

The function  $E_{\alpha,\beta}(-t)$ ,  $t \geq 0$ , is known to be completely monotone for  $0 < \alpha \leq 1$ ,  $\beta \geq \alpha$ . However, this monotonicity is not necessarily preserved when  $(\alpha, \beta) \in \Omega$  since

either the function or its derivative could have roots. On the other hand, it has been established in [20] that  $E_{\alpha,\beta}$  has at most a finite number of roots when  $(\alpha, \beta) \in \Omega$ . Thus,  $E_{\alpha,\beta}(-t)$  is monotone for sufficiently large  $t$ . Furthermore, it is shown in [20] that there exists only one zero when  $\alpha$  is sufficiently close to 1 while the number of zeros increases as  $\alpha$  increases towards 2.

In Figure 1, the curve  $\phi$  is the boundary given in [20, Table 1] such that  $E_{\alpha,\beta}$  has a finite number of real roots when  $(\alpha, \beta)$  is below it and none above it. However, the function in the region below  $\phi(\alpha)$  differs with respect to the number of roots. Typically, the number of roots increases as  $\alpha$  goes to 2. Similarly, we constructed the boundary  $\psi$  for the derivative. The corresponding data is presented in Table 1.

The monotonicity and oscillatory behavior of  $E_{\alpha,\beta}$  is characterized by the different regions marked in Figure 1 and described in Table 2. It follows from (4) that  $E_{\alpha,\beta}(-t)$  is monotonically decreasing for  $(\alpha, \beta)$  in the regions (D) and (F). In the regions (B) and (C), although the function has no real roots, it could have a finite number of oscillations due to the roots of the derivative.

**Remark.** Since  $E_{\alpha,\beta}(-t) \rightarrow 0$  as  $t \rightarrow \infty$ , it is obvious that each root of it is followed by at least one root of its derivative. This is consistent with the inequality

$$\phi(\alpha) < \psi(\alpha).$$

For the region below the line  $\beta = \alpha + 1$ , which includes the regions (A), (B) and (D), the following decomposition is presented in [19],

$$E_{\alpha,\beta}(-t) = g_{\alpha,\beta}(-t) + f_{\alpha,\beta}(-t), \quad t > 0, \quad \beta < \alpha + 1, \quad (5)$$

where the function  $f_{\alpha,\beta}(-t)$  is asymptotically approaching zero as  $t \rightarrow \infty$  and  $g_{\alpha,\beta}(-t)$  is an oscillatory function.

When  $\beta = 1$  and  $1 < \alpha < 2$ , the function  $f_{\alpha,1}(-t)$  is known to be a completely monotonic function while the function  $g_{\alpha,1}(-t)$  is oscillatory with exponentially decreasing amplitude [3]. The properties of  $E_{\alpha}$ ,  $1 < \alpha < 2$ , such as monotonicity, roots, and the oscillatory behavior have been discussed in details in [23].

In the region (B), although  $E_{\alpha,\beta}(-t)$  has no roots as it decays to zero, it undergoes oscillations due to the roots of its derivative as demonstrated in Figure 2. This behavior is also consistent with the oscillatory nature of  $g_{\alpha,\beta}$  there. On the other hand, in the region (D) in which  $E_{\alpha,\beta}$  is monotone, the behavior of the oscillatory function  $g_{\alpha,\beta}$  fades away and  $f_{\alpha,\beta}(-t)$  dominates.

### 3. Derooting decomposition

A key step to accurately approximate  $E_{\alpha,\beta}(-t)$  when  $1 < \alpha < 2$  is to capture its oscillatory behavior and roots. However, in region (A) the number of roots in general

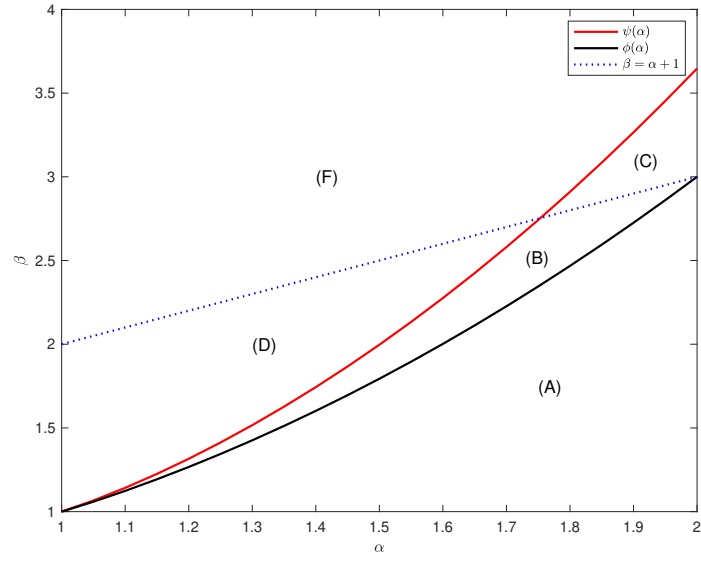


Figure 1:  $\alpha$ - $\beta$  phase diagram for  $E_{\alpha,\beta}(-t)$  and its derivative.

Table 1: The data for the boundaries  $\phi$  and  $\psi$ .

$\alpha$	$\phi(\alpha)$	$\psi(\alpha)$
1.00	1.00000	1.00000
1.05	1.05924	1.06640
1.10	1.12400	1.14204
1.15	1.19325	1.22532
1.20	1.26674	1.31565
1.25	1.34437	1.41277
1.30	1.42608	1.51654
1.35	1.51187	1.62689
1.40	1.60173	1.74374
1.45	1.69565	1.86706
1.50	1.79365	1.99685
1.55	1.89573	2.13306
1.60	2.00191	2.27568
1.65	2.11219	2.42471
1.70	2.22660	2.58014
1.75	2.34513	2.74196
1.80	2.46779	2.91017
1.85	2.59460	3.08477
1.90	2.72557	3.26575
1.95	2.86070	3.45311
2.00	3.00000	3.64686

Table 2: Number of roots in the regions of Figure 1.

Region	$E_{\alpha,\beta}(-t)$	$dE_{\alpha,\beta}/dt$
A	Finite number of roots	Finite number of roots
B	No real roots	Finite number of roots
C	No real roots	Finite number of roots
D	No real roots	No real roots
F	No real roots	No real roots

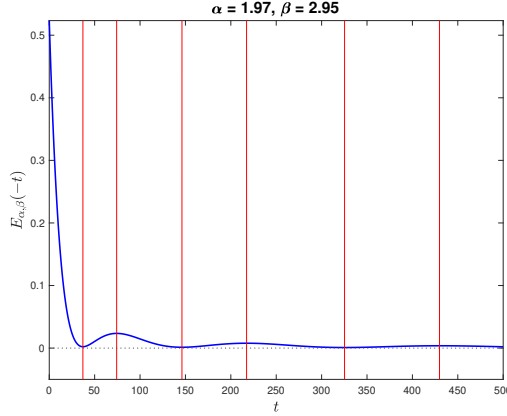


Figure 2: Typical oscillations in region (B) about the roots (marked by the red lines) of the derivative.

could exceed the ones of rational approximants. This makes these approximants valid only for small arguments.

A Derooting approach can be used to extend the validity of rational approximants to large intervals. For this purpose, we use the following recursive identity [24]

$$E_{\alpha,\beta}(t) = t^r E_{\alpha,\beta+\alpha r}(t) + P_{\alpha,\beta}^{r-1}(t), \quad (6)$$

$$\alpha > 0, \quad \beta > 0, \quad t \in \mathbb{R}, \quad r = 0, 1, 2, \dots,$$

where,

$$P_{\alpha,\beta}^{r-1}(t) := \begin{cases} \sum_{k=0}^{r-1} \frac{t^k}{\Gamma(\alpha k + \beta)}, & r = 1, 2, 3, \dots \\ 0, & r = 0. \end{cases} \quad (7)$$

In this identity,  $E_{\alpha,\beta}$  is decomposed into another MLF with shifted second parameter and a polynomial of degree  $r - 1$ . This allows us to replace the parameters  $(\alpha, \beta)$  in region (A) by parameters  $(\alpha, \beta + \alpha r)$  above the boundaries  $\phi(\alpha)$  or above  $\psi(\alpha)$ . Consequently, we obtain a function  $E_{\alpha,\beta+\alpha r}$  that has no roots or even could be monotone. Therefore, the approximation of  $E_{\alpha,\beta}(-t)$ ,  $1 < \alpha < 2$ , with a finite number of real roots can be replaced by approximating another one that has no roots or one that is monotone.

## 4. Rational approximation

Based on the global rational approximation technique introduced for transcendental functions in [15], a variety of global Padé approximants for  $E_{\alpha,\beta}(-t)$ ,  $0 < \alpha < 1$ , are developed and implemented [16, 17, 18, 10, 11]. These approximants are still valid for  $E_{\alpha,\beta}(-t)$ ,  $1 < \alpha < 2$ , over intervals in which the number of its roots does not exceed the number of approximant roots. This renders these approximants inadequate when approximating MLF over an interval in which it has multiple roots, as the case when  $(\alpha, \beta)$  in region (A) of Figure 1.

In this section we consider the global Padé approximants  $R_{\alpha,\beta}^{7,2}$  and  $R_{\alpha,\beta}^{13,4}$  developed in [10, 11] and examine their performance when  $1 < \alpha < 2$ . Then we describe how the derooting decomposition leads to approximants with increased number of roots and thus able to track more of MLF roots.

### 4.1. Global Padé approximation

For  $\{(\alpha, \beta) : 1 < \alpha < 2, \beta \geq 1, \alpha \neq \beta\}$ , we consider the global Padé approximants

$$R_{\alpha,\beta}^{7,2}(t) = \frac{1}{\Gamma(\beta - \alpha)} \frac{p_1 + p_2 t + p_3 t^2 + t^3}{q_0 + q_1 t + q_2 t^2 + q_3 t^3 + t^4}, \quad t \geq 0, \quad (8)$$

and

$$R_{\alpha,\beta}^{13,4}(t) = \frac{1}{\Gamma(\beta - \alpha)} \frac{p_1 + p_2 t + \dots + p_7 t^6 + t^7}{q_0 + q_1 t + q_2 t^2 + \dots + q_7 t^7 + t^8}, \quad t \geq 0, \quad (9)$$

where the coefficients satisfy respectively the systems

$$\begin{pmatrix} 1 & 0 & 0 & a_0 & 0 & 0 & 0 \\ 0 & 1 & 0 & a_1 & a_0 & 0 & 0 \\ 0 & 0 & 1 & a_2 & a_1 & a_0 & 0 \\ 0 & 0 & 0 & a_3 & a_2 & a_1 & a_0 \\ 0 & 0 & 0 & a_4 & a_3 & a_2 & a_1 \\ 0 & 0 & 0 & a_5 & a_4 & a_3 & a_2 \\ 0 & 0 & 1 & 0 & 0 & 0 & b_0 \end{pmatrix} \begin{pmatrix} p_1 \\ p_2 \\ p_3 \\ q_0 \\ q_1 \\ q_2 \\ q_3 \end{pmatrix} = \begin{pmatrix} 0 \\ 0 \\ 0 \\ -1 \\ -a_0 \\ -a_1 \\ -b_1 \end{pmatrix},$$

$$\begin{pmatrix}
1 & 0 & 0 & 0 & 0 & 0 & 0 & 0 & a_0 & 0 & 0 & 0 & 0 & 0 & 0 & 0 \\
0 & 1 & 0 & 0 & 0 & 0 & 0 & 0 & a_1 & a_0 & 0 & 0 & 0 & 0 & 0 & 0 \\
0 & 0 & 1 & 0 & 0 & 0 & 0 & 0 & a_2 & a_1 & a_0 & 0 & 0 & 0 & 0 & 0 \\
0 & 0 & 0 & 1 & 0 & 0 & 0 & 0 & a_3 & a_2 & a_1 & a_0 & 0 & 0 & 0 & 0 \\
0 & 0 & 0 & 0 & 1 & 0 & 0 & 0 & a_4 & a_3 & a_2 & a_1 & a_0 & 0 & 0 & 0 \\
0 & 0 & 0 & 0 & 0 & 1 & 0 & 0 & a_5 & a_4 & a_3 & a_2 & a_1 & a_0 & 0 & 0 \\
0 & 0 & 0 & 0 & 0 & 0 & 1 & 0 & a_6 & a_5 & a_4 & a_3 & a_2 & a_1 & a_0 & 0 \\
0 & 0 & 0 & 0 & 0 & 0 & 0 & 0 & a_7 & a_6 & a_5 & a_4 & a_3 & a_2 & a_1 & a_0 \\
0 & 0 & 0 & 0 & 0 & 0 & 0 & 0 & a_8 & a_7 & a_6 & a_5 & a_4 & a_3 & a_2 & a_1 \\
0 & 0 & 0 & 0 & 0 & 0 & 0 & 0 & a_9 & a_8 & a_7 & a_6 & a_5 & a_4 & a_3 & a_2 \\
0 & 0 & 0 & 0 & 0 & 0 & 0 & 0 & a_{10} & a_9 & a_8 & a_7 & a_6 & a_5 & a_4 & a_3 \\
0 & 0 & 0 & 0 & 0 & 0 & 0 & 0 & a_{11} & a_{10} & a_9 & a_8 & a_7 & a_6 & a_5 & a_4 \\
0 & 0 & 0 & 0 & 1 & 0 & 0 & 0 & 0 & 0 & 0 & 0 & 0 & b_0 & b_1 & b_2 \\
0 & 0 & 0 & 0 & 0 & 1 & 0 & 0 & 0 & 0 & 0 & 0 & 0 & 0 & b_0 & b_1 \\
0 & 0 & 0 & 0 & 0 & 0 & 0 & 0 & 0 & 0 & 0 & 0 & 0 & 0 & 0 & b_0
\end{pmatrix}
\begin{pmatrix}
p_1 \\ p_2 \\ p_3 \\ p_4 \\ p_5 \\ p_6 \\ p_7 \\ q_0 \\ q_1 \\ q_2 \\ q_3 \\ q_4 \\ q_5 \\ q_6 \\ q_7
\end{pmatrix}
=
\begin{pmatrix}
0 \\ 0 \\ 0 \\ 0 \\ 0 \\ 0 \\ 0 \\ -1 \\ -a_0 \\ -a_1 \\ -a_2 \\ -a_3 \\ -a_4 \\ -b_3 \\ -b_2 \\ -b_1
\end{pmatrix},$$

$$a_j = \frac{(-1)^{j+1}\Gamma(\beta - \alpha)}{\Gamma(\beta + j\alpha)}, \quad b_j = \frac{(-1)^{j+1}\Gamma(\beta - \alpha)}{\Gamma(\beta - (j + 1)\alpha)}, \quad j = 0, 1, \dots$$

Computationally, it is observed that  $R_{\alpha,\beta}^{13,4}$  has at most three real roots, while  $R_{\alpha,\beta}^{7,2}$  has exactly one real root. Consequently, in approximating some of the oscillatory MLFs, each approximant is only able to trace the function up to its largest root. To illustrate the accuracy and limitations of both approximants when  $1 < \alpha < 2$ , we compare with the Matlab routine `ml` [9] and `ml_matrix` [22].

In Figure 3, two examples from region (A) are shown. In plot (a), the MLF has only one root which is typically the case for  $1 < \alpha < 1.4$ . As observed,  $R_{\alpha,\beta}^{13,4}$  provides a good approximation in this cases. In plot (b), the MLF has many roots which typically the case as  $\alpha$  gets closer to 2. As expected, each approximant fails beyond its largest root to capture the oscillations of the MLF.

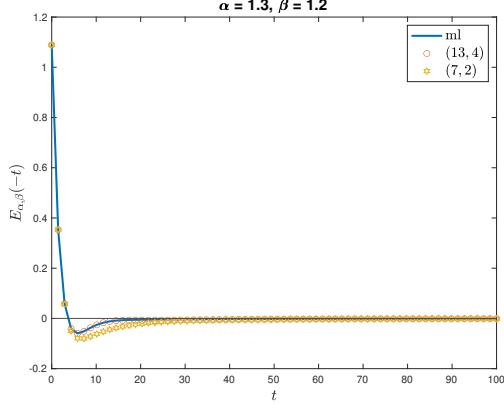
In Figure 4, typical cases from Region (B) and (C) are shown. The corresponding MLFs in both regions is root-free but are oscillatory. As shown,  $R_{\alpha,\beta}^{13,4}$  is sufficiently accurate for an extended interval. However, eventually it takes negative values as observed in plot (b).

In Figure 5, typical cases from regions (D) and (F) are illustrated. In both regions the MLF is monotone and globally positive. As seen clearly,  $R_{\alpha,\beta}^{13,4}$  is a good approximation for an extended interval.

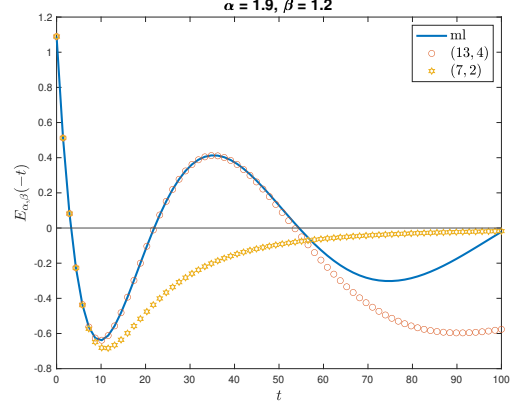
As general guidelines, we have the following.

- When  $(\alpha, \beta)$  in Regions (A), the existing global Padé approximants are not effective over extended intervals due to the existence of roots.
- When  $(\alpha, \beta)$  in region (B) or (C), more accurate approximants should be used due to the oscillatory behavior of MLF.



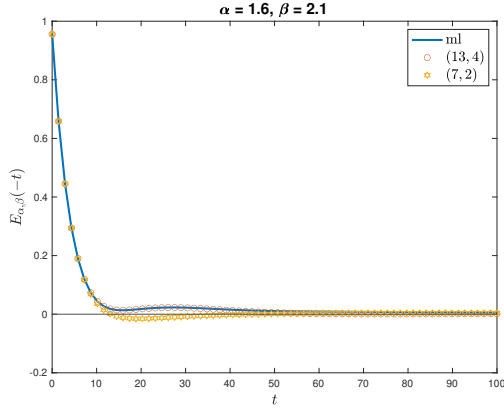


(a) Region(A): one root

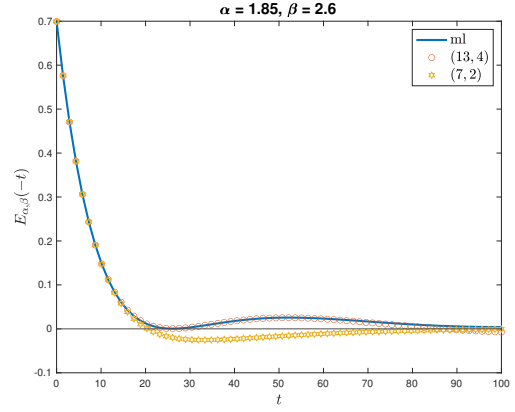


(b) Region(A): many roots

Figure 3: Plots of  $R_{\alpha,\beta}^{13,4}$  and  $R_{\alpha,\beta}^{7,2}$  approximants of  $E_{\alpha,\beta}$ ,  $(\alpha, \beta)$  in region (A).

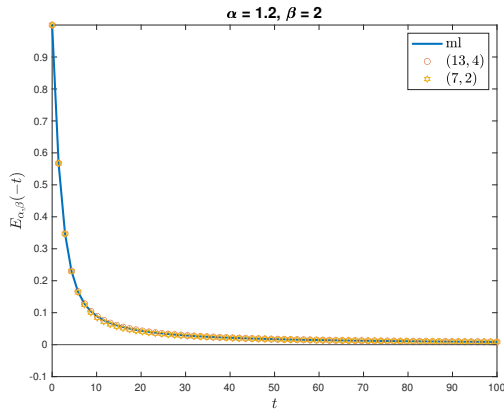


(a) Region(B): no roots and oscillatory

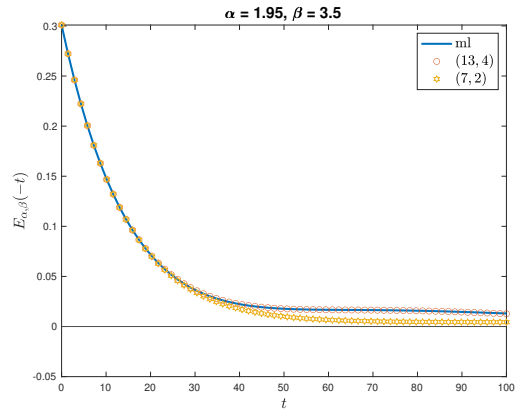


(b) Region(C): no roots and oscillatory

Figure 4: Plots of  $R_{\alpha,\beta}^{13,4}$  and  $R_{\alpha,\beta}^{7,2}$  approximants of  $E_{\alpha,\beta}$ ,  $(\alpha, \beta)$  in regions (B) and (C).



(a) Region(D): monotone and positive



(b) Region(F): monotone and positive

Figure 5: Plots of  $R_{\alpha,\beta}^{13,4}$  and  $R_{\alpha,\beta}^{7,2}$  approximants of  $E_{\alpha,\beta}$ ,  $(\alpha, \beta)$  in regions (D) and (F).

- When  $(\alpha, \beta)$  in Region (D) or (F), the approximant  $R_{\alpha, \beta}^{13,4}$  is sufficiently accurate since MLF is globally monotone.

#### 4.2. Rational approximation for oscillatory MLFs

As observed in the above subsection, when  $(\alpha, \beta)$  lies below the boundary  $\psi(\alpha)$  in Figure 1, then more accurate and multi roots approximants are essential for extended intervals. Next, we propose a class of rational approximants that have the desirable performance.

It follows from (6) that we can write

$$E_{\alpha, \beta}(-t) = (-t)^r E_{\alpha, \beta + \alpha r}(-t) + P_{\alpha, \beta}^{r-1}(-t), \quad t > 0.$$

Let  $R_{\alpha, \beta}^{m, n}$  be the global Padé approximants described in [10]. We introduce the rational approximant

$$E_{\alpha, \beta}(-t) \approx R_{\alpha, \beta}^{m, n, r}(t), \quad t > 0, \quad (10)$$

where,

$$R_{\alpha, \beta}^{m, n, r}(t) := (-t)^r R_{\alpha, \beta + \alpha r}^{m, n}(t) + P_{\alpha, \beta}^{r-1}(-t), \quad r = 0, 1, 2, \dots \quad (11)$$

Note that as a special case we have

$$R_{\alpha, \beta}^{m, n, 0} = R_{\alpha, \beta}^{m, n}.$$

The integer  $r$  could be chosen so that  $(\alpha, \beta + \alpha r)$  lies above the boundary  $\psi(\alpha)$  in Figure 1. As demonstrated in the previous subsection, this shifting of parameters would enhance the performance of  $R_{\alpha, \beta + \alpha r}^{m, n}$  since in this case  $E_{\alpha, \beta + \alpha r}(-t)$  is root-free and non-oscillatory. Furthermore,  $r$  could be chosen large enough so that the approximant  $R_{\alpha, \beta}^{m, n, r}$  captures the desired number of roots and oscillations of  $E_{\alpha, \beta}$  over an extended interval.

The performance of the generalized approximant  $R_{\alpha, \beta}^{13,4,r}$  when  $(\alpha, \beta)$  in regions (A) and (C) is demonstrated in Figures 6 and 7, respectively, where

$$|e_{\alpha, \beta}^{m, n, r}(t)| := |E_{\alpha, \beta}(-t) - R_{\alpha, \beta}^{m, n, r}(t)|.$$

As can be observed, the interval of approximation can be extended by increasing  $r$ . The generalized approximant  $R_{\alpha, \beta}^{7,2,r}$  has the same features, although it is not as accurate as  $R_{\alpha, \beta}^{14,3,r}$ , as shown in Figure 8.

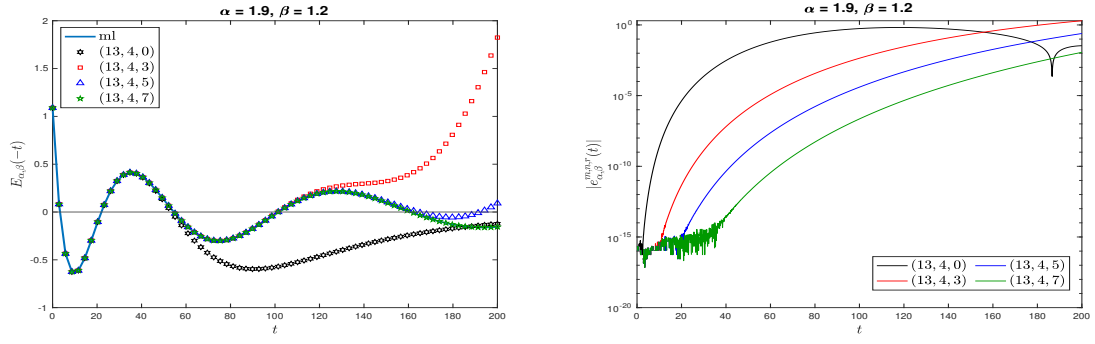


Figure 6: Plots of  $R_{\alpha,\beta}^{13,4,r}$  for different values of  $r$  when  $(\alpha, \beta)$  in region (A).

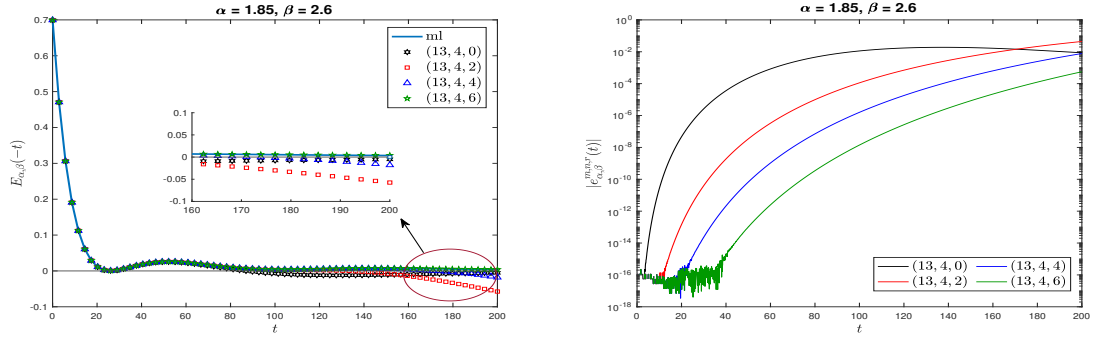


Figure 7: Plots of  $R_{\alpha,\beta}^{13,4,r}$  for different values of  $r$  when  $(\alpha, \beta)$  in region (C).

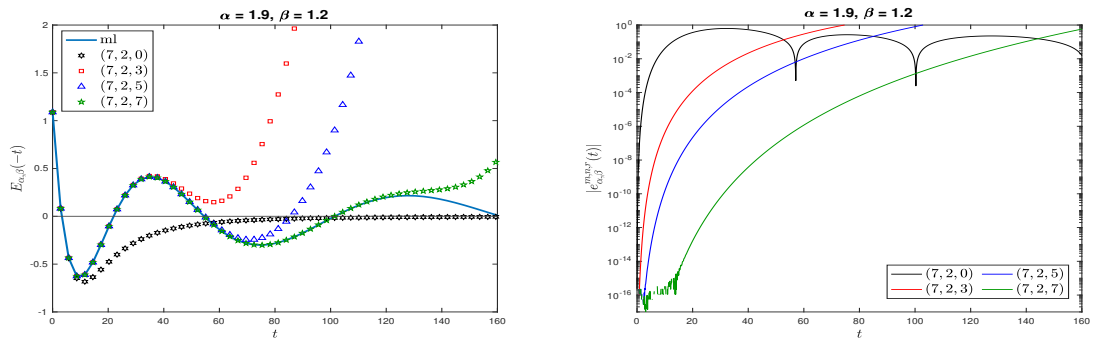


Figure 8: Plots of  $R_{\alpha,\beta}^{7,2,r}$  for different values of  $r$  when  $(\alpha, \beta)$  in region (A).

## 5. Approximation of matrix Mittag-Leffler

In this section we study the approximation of matrix MLF defined by [25]

$$E_{\alpha,\beta}(A) = \sum_{k=0}^{\infty} \frac{A^k}{\Gamma(\alpha k + \beta)}, \quad \operatorname{Re} \alpha > 0, \beta \in \mathbb{C}, \quad A \in \mathbb{C}^{n \times n}. \quad (12)$$

Using the definition of rational functions of matrices, see [26], we define the global Padé approximation of  $E_{\alpha,\beta}(A)$  by

$$R_{\alpha,\beta}^{m,n}(A) := \frac{1}{\Gamma(\beta - \alpha)} [q(A)]^{-1} p(A), \quad (13)$$

for some appropriate matrix  $A$ , where  $p$  and  $q$  denote the numerator and denominator, respectively, of  $\Gamma(\beta - \alpha)R_{\alpha,\beta}^{m,n}$ . Furthermore, by extending the decomposition (6) to matrix arguments, we define the rational approximant

$$R_{\alpha,\beta}^{m,n,r}(A) := (-A)^r R_{\alpha,\beta+r\alpha}^{m,n}(A) + P_{\alpha,\beta}^{r-1}(-A), \quad r = 0, 1, 2, \dots, \quad (14)$$

where  $P_{\alpha,\beta}^{r-1}$  is the polynomial given by (7).

Next we discuss some approaches for implementing (13) and compare their accuracy and computation time.

### 1. Matrix Inversion approach

In this approach the inverse of  $q(A)$  is calculated and then substituted in (13).

### 2. Linear System approach

The approximant  $R_{m,n}^{\alpha,\beta}(A)$  is obtained by solving the matrix system

$$q(A)R_{m,n}^{\alpha,\beta}(A) = p(A).$$

This requires solving  $N$  systems for an  $N \times N$  matrix.

### 3. Partial Fraction approach

Partial fraction decomposition is known to provide an efficient form for evaluating rational functions. For the global Padé approximants, it has been discussed in [10, 11] that these approximants have complex conjugate roots which can add to the efficient implementation. As an example, the approximant  $R_{\alpha,\beta}^{13,4}(x)$  which admits the partial fraction decomposition

$$R_{\alpha,\beta}^{13,4}(x) = \sum_{i=1}^4 \left[ \frac{c_i}{x - s_i} + \frac{\bar{c}_i}{x - \bar{s}_i} \right], \quad (15)$$

where  $\{c_1, c_2, c_3, c_4\}$  and  $\{s_1, s_2, s_3, s_4\}$  are the non-conjugate residues and poles, respectively, can be written as

$$R_{\alpha,\beta}^{13,4}(x) = 2 \operatorname{Re} \sum_{i=1}^4 \left[ \frac{c_i}{x - s_i} \right]. \quad (16)$$

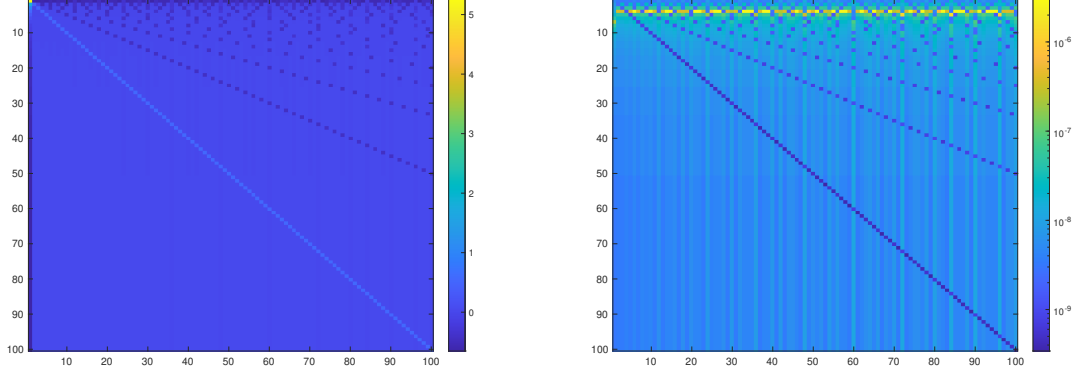


Figure 9: MLF matrix approximation  $R_{\alpha,\beta}^{13,4}$ ,  $(\alpha, \beta) = (1.9, 1)$ , of  $100 \times 100$  Redheffer matrix using partial fractions (Left) and its relative error (Right).

So for a matrix argument  $A$ , the approximant can be calculated as

$$E_{\alpha,\beta}(-A) \approx R_{\alpha,\beta}^{13,4}(A) := 2 \operatorname{Re} \sum_{j=1}^4 c_j (A - s_j I)^{-1},$$

where  $I$  is the identity matrix.

#### 4. Matrix Diagonalization approach

When the matrix argument  $A$  is diagonalizable, then the factorization  $A = Z D Z^{-1}$  could be considered, where  $D$  is the diagonal matrix containing the eigenvalues and the columns of  $Z$  are the corresponding eigenvectors. In this case, the Matrix MLF can be computed as

$$E_{\alpha,\beta}(A) = Z E_{\alpha,\beta}(D) Z^{-1} = Z \operatorname{diag}(E_{\alpha,\beta}(\lambda_i)) Z^{-1}.$$

Accordingly, the approximant  $R_{\alpha,\beta}^{m,n}$  could be computed as

$$R_{\alpha,\beta}^{m,n}(A) = Z \operatorname{diag}(R_{\alpha,\beta}^{m,n}(\lambda_i)) Z^{-1}.$$

For experimental purposes, we consider the performance of the approximant (11) when applied to Redheffer matrix of size  $100 \times 100$ , in comparison to the reference values by `ml_matrix`. In Figure 9, a color map is showing the component-wise values and relative errors for  $R_{\alpha,\beta}^{13,4}$ ,  $(\alpha, \beta) = (1.9, 1)$ , when calculated using partial fractions. In Table 3, a comparison of the absolute error, relative error, and runtime is provided for the different techniques in computing  $R_{\alpha,\beta}^{13,4}$ .

## 6. Applications and numerical experiments

We present here some applications of the general Padé approximant (11) related to fractional oscillation equations where MLFs arise naturally as solutions. Numerical experiments are included to highlight the efficiency and accuracy of these approximants.

Table 3: Maximum absolute error (AE), maximum relative error (RE) and the runtime (in seconds) for computing the matrix MLF of a  $100 \times 100$  Redheffer matrix,  $\beta = 1$ .

	$\alpha = 1.5$			$\alpha = 1.9$		
	AE	RE	Runtime	AE	RE	Runtime
Matrix Inversion	1.13E-04	7.20E-03	2.00E-03	2.41E-08	3.00E-06	1.10E-03
Linear System	1.13E-04	7.20E-03	1.90E-03	2.41E-08	3.00E-06	1.10E-03
Partial Fraction	1.13E-04	7.20E-03	3.70E-03	2.41E-08	3.00E-06	2.30E-03
ml_matrix			1.44E-01			9.73E+00

### 6.1. Application: Fractional plasma oscillations

The fractional plasma oscillation model, as in [27], is given by

$$\begin{aligned} {}^c D^\alpha u(t) + Au(t) &= f(t), \\ u(0) &= u_0, \\ u'(0) &= u_1, \end{aligned} \tag{17}$$

where  ${}^c D^\alpha$  denotes the Caputo fractional derivative of order  $\alpha \in (1, 2)$  defined by

$${}^c D^\alpha u(t) := \begin{cases} \frac{1}{\Gamma(2-\alpha)} \int_0^t (t-\tau)^{1-\alpha} u''(\tau) d\tau, & 1 < \alpha < 2, \\ u''(t), & \alpha = 2. \end{cases}$$

The constant  $A$  is the fractional electron plasma frequency and  $f(t)$  is the electric field. We consider the model with static electric field and with no electric field.

#### 6.1.1. Fractional plasma oscillations model with static electric field

Consider the special case of problem (17),

$${}^c D^\alpha u(t) + u(t) = 1, \quad u(0) = 1, \quad u'(0) = -1.$$

The exact solution for this initial value problem is

$$u(t) = E_\alpha(-t^\alpha) - tE_{\alpha,2}(-t^\alpha) + t^\alpha E_{\alpha,\alpha+1}(-t^\alpha). \tag{18}$$

In Figure 10, a comparison of approximations of (18) when  $\alpha = 1.2$  is provided. Considering the three terms in (18), the pair  $(\alpha, \beta)$  when  $\beta = 1$  falls in region (A) of the phase diagram 1, where the MLF is oscillatory. While the pairs  $(1.2, 2)$  and  $(1.2, 2.2)$  fall in region (D) and (F), respectively, in which the MLF has no real roots and no oscillations. A similar comparison when  $\alpha = 1.9$  is included in Figure 11. In this case, the terms  $E_{1.9,1}$  and  $E_{1.9,2}$  correspond to  $(\alpha, \beta)$  in parts of Region (A) in which the MLF is highly oscillatory and has many real roots.

Table 4: Maximum relative error (RE) and runtime in computing the solution (18), over the time mesh  $[0, 0.17, 0.34, \dots, 17]$ ,  $\alpha = 1.9$ .

	RE	Runtime
$R_{\alpha,\beta}^{13,4}$	1.56E+00	5.69E-04
$R_{\alpha,\beta}^{13,4,2}$	4.59E+00	5.19E-04
$R_{\alpha,\beta}^{13,4,5}$	7.56E-01	5.20E-04
$R_{\alpha,\beta}^{13,4,8}$	9.91E-03	5.52E-04
ml	-	2.38E-02

To illustrate the computation efficiency, it is seen in Table 4 that  $R_{\alpha,\beta}^{13,4}$  and  $R_{\alpha,\beta}^{13,4,r}$  with  $r = 2, 5, 8$  have significantly less computation cost (in time) than the ml function. Moreover, while the modified approximant  $R_{\alpha,\beta}^{13,4,8}$  yields more accurate approximations than  $R_{\alpha,\beta}^{13,4}$  when compared to the reference values, they have comparable computation time.

### 6.1.2. Fractional plasma oscillations model with no electric field

Consider the initial values problem

$${}^c D^\alpha u(t) + u(t) = 0, \quad u(0) = 0.2, \quad u'(0) = 0.1.$$

The exact solution of this problem is given by

$$u(t) = 0.2E_\alpha(-t^\alpha) + 0.1tE_{\alpha,2}(-t^\alpha). \quad (19)$$

A comparison of approximations of (19) when  $\alpha = 1.9$  is provided in Figure 12. Unlike the static electric field case, it is observed that over an extended time interval, the solution of the fractional oscillation equation has more oscillations around zero. To sufficiently capture these oscillations on the interval  $[0, 20]$ , the approximant  $R_{\alpha,\beta}^{13,4,15}$  can be used.

### 6.2. Application: Time fractional diffusion-wave equation

Consider the fractional diffusion-wave problem, [28]:

$$\begin{aligned} {}^c \partial_t^\alpha u(x, t) &= \partial_x^2 u(x, t), \quad 0 \leq x \leq \pi, \\ u(x, 0) &= \sin(x), \\ \partial_t u(x, t)|_{t=0} &= 0, \\ u(0, t) &= u(\pi, t) = 0, \quad t \in (0, T], \end{aligned} \quad (20)$$

where  ${}^c \partial_t^\alpha$  and  $\partial_t$  are the fractional partial time derivative of order  $\alpha \in (1, 2)$  and first partial derivative in  $t$ , respectively, and  $\partial_x^2$  is the second partial derivative in space.

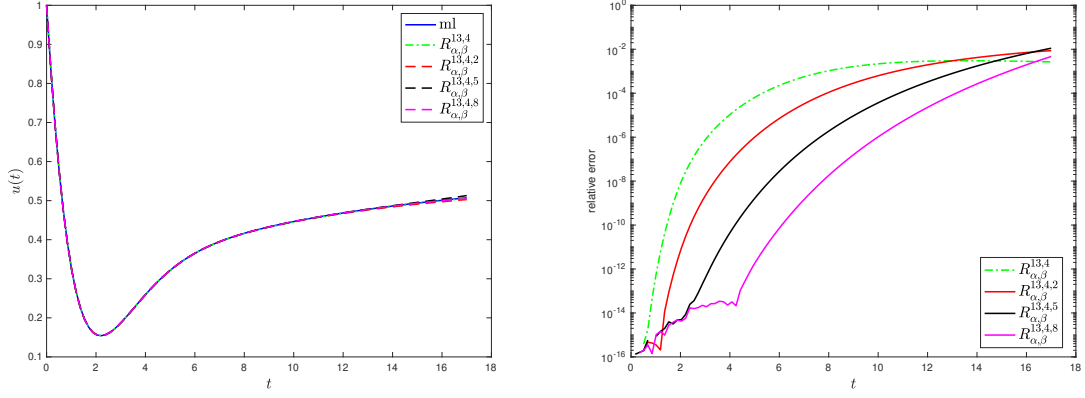


Figure 10: Profiles (left) and relative error (right) in approximating the solution (18),  $\alpha = 1.2$ .

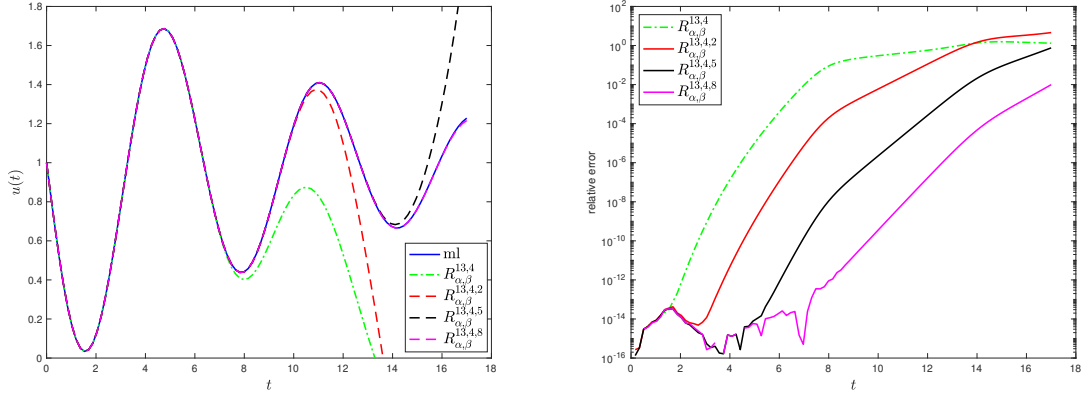


Figure 11: Profiles (left) and relative error (right) in approximating the solution (18),  $\alpha = 1.9$ .

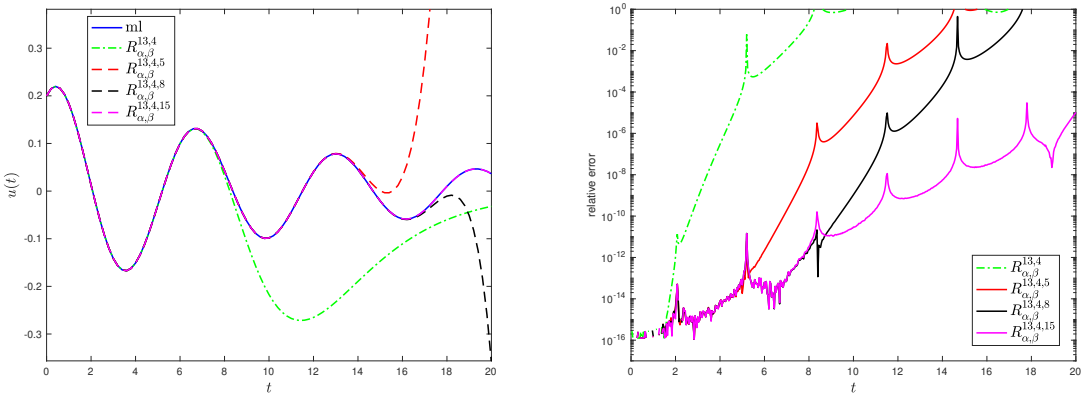


Figure 12: Profiles (left) and relative error (right) in approximating the solution (19),  $\alpha = 1.9$ .



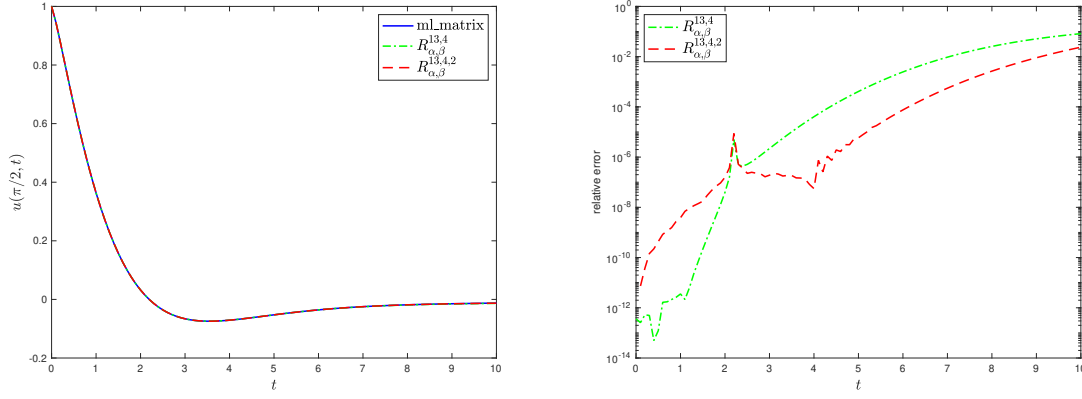


Figure 13: Application 6.2: approximation of  $u(\pi/2, t)$  (left) and relative error (right),  $\alpha = 1.2$ .

The exact solution of (20) is  $u(x, t) = E_\alpha(-t^\alpha) \sin(x)$ , however, this problem is intended to illustrate the performance of the approximants (11). To this end, applying the second central difference approximation to (20) over uniform spatial mesh with step size  $h = \pi/(m+1)$ , leads to a system of the form

$$\begin{aligned} {}^c D^\alpha U(t) + AU(t) &= 0, \quad t > 0, \\ U(0) &= U_0, \\ U'(0) &= 0, \end{aligned} \tag{21}$$

where the  $m \times m$  matrix  $A = [a_{ij}]$  is tridiagonal with  $a_{i,i} = 2$  and  $a_{i,j} = -1$  for  $j = i \pm 1$ . Further,  $U(t) = [u_1(t), u_2(t), \dots, u_m(t)]^T$ ,  $U(0) = [\sin(x_1), \sin(x_2), \dots, \sin(x_m)]^T$ , where  $u_1(t) = u(x_1, t)$  and  $x_i = i \times \pi/m$ . The solution of the above system of differential equations is given by  $U(t) = E_\alpha(-At^\alpha)U_0$ . As an experiment, we take  $h = \pi/100$ , so the coefficient matrix  $A$  is of size  $99 \times 99$ . In addition, the rational approximation of the matrix MLF is computed by the diagonalization approach.

In Figure 13, the solution profile is presented for the case  $\alpha = 1.2$ . As can be seen, both the global Padé approximant  $R_{1.2,1}^{13,4}$  and its generalization  $R_{1.2,1}^{13,4,2}$  are comparable. This is expected since the solution has only one root and not much oscillatory behavior is experienced. In Figure 14, the case  $\alpha = 1.9$  where the MLF is more oscillatory is presented. In this case the rational approximant  $R_{1.9,1}^{13,4}$  fails to capture the oscillations for large  $t$  and thus yields undesirable approximations. However, the modified  $R_{1.9,1}^{13,4,r}$  with an appropriate choice  $r = 2$  rectifies this issue and gives more accurate approximate values.

To illustrate the efficiency of these approximants, their runtime is compared with that of `ml_matrix` Matlab function. Table 5 includes the CPU time for computing the solution  $U(t) = E_\alpha(-At^\alpha)U_0$  on a time mesh  $\{t_n = 0.1n, n = 0, 1, \dots, 100\}$  as well as the maximum relative error between the approximate and reference values. The results show that the approximant  $R_{1.9,1}^{13,4,2}$  performs about seven times faster than the `ml_matrix`. Moreover, while the approximant  $R_{1.9,1}^{13,4,2}$  on an extended interval is able to achieve higher accuracy than  $R_{1.9,1}^{13,4}$ , their runtime is comparable.

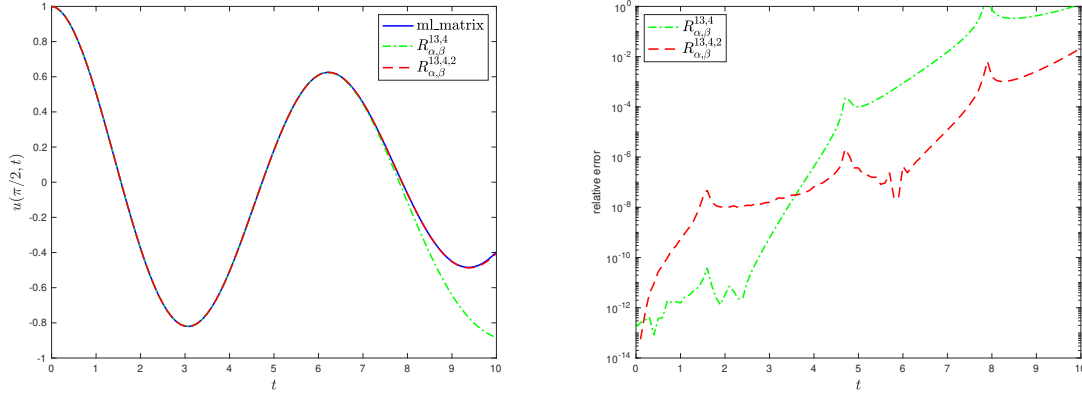


Figure 14: Application 6.2: approximation of  $u(\pi/2, t)$  (left) and relative error (right),  $\alpha = 1.9$ .

Table 5: Application 6.2: maximum relative error (RE) and runtime in computing the solution of (21) over the time mesh  $[0, 0.1, 0.2, \dots, 10]$ ,  $\alpha = 1.9$ .

	RE	Runtime
$R_{1.9,1}^{13,4}$	3.38E+00	8.00E-02
$R_{1.9,1}^{13,4,2}$	2.20E-02	9.95E-02
ml_matrix	-	6.796E-01

## 7. Concluding Remarks

In this paper, a characterization of the oscillatory and monotone behavior of two-parameter Mittag-Leffler function is given. Furthermore, generalized rational approximants over extended intervals are developed. These approximants are based on decomposing Mittag-Leffler function into a root-free one and a polynomial. The approximants have good tracking capabilities of the roots and oscillations over extended intervals. Such approximants play an effective role in the implementation of numerical methods for fractional oscillation equations.

## References

- [1] A. Kilbas, H. Srivastava, and J. Trujillo, *Theory and applications of fractional differential equations*. Elsevier, 2006.
- [2] R. Gorenflo, A. A. Kilbas, F. Mainardi, and S. V. Rogosin, *Mittag-Leffler functions. related topics and applications*. Springer, 2014.
- [3] R. Gorenflo and F. Mainardi, *Fractional oscillations and Mittag-Leffler functions*. Citeseer, 1996.
- [4] F. Mainardi, “Fractional relaxation-oscillation and fractional diffusion-wave phenomena,” *Chaos, Solitons & Fractals*, vol. 7, no. 9, pp. 1461–1477, 1996.

- [5] B. N. Achar, J. Hanneken, T. Enck, and T. Clarke, “Dynamics of the fractional oscillator,” *Physica A: Statistical Mechanics and its Applications*, vol. 297, no. 3-4, pp. 361–367, 2001.
- [6] A. Stanislavsky, “Fractional oscillator,” *Physical review E*, vol. 70, no. 5, p. 051103, 2004.
- [7] A. A. Stanislavsky, “Twist of fractional oscillations,” *Physica A: Statistical Mechanics and its Applications*, vol. 354, pp. 101–110, 2005.
- [8] R. Gorenflo, J. Loutchko, and Y. Luchko, “Computation of the Mittag-Leffler function  $E_{\alpha,\beta}(z)$  and its derivative,” *Fractional Calculus & Applied Analysis*, vol. 5, no. 4, pp. 491–518, 2002.
- [9] R. Garrappa, “Numerical evaluation of two and three parameter Mittag-Leffler functions,” *SIAM Journal on Numerical Analysis*, vol. 53, no. 3, pp. 1350–1369, 2015.
- [10] I. O. Sarumi, K. M. Furati, and A. Q. M. Khaliq, “Highly accurate global Padé approximations of generalized Mittag-Leffler function and its inverse,” *Journal of Scientific Computing*, vol. 82, no. 46, 2020.
- [11] I. O. Sarumi, K. M. Furati, A. Q. M. Khaliq, and K. Mustapha, “Generalized exponential time differencing schemes for stiff fractional systems with nonsmooth source term,” *Journal of Scientific Computing*, vol. 86, no. 23, 2021.
- [12] O. S. Iyiola, E. O. Asante-Asamani, and B. A. Wade, “A real distinct poles rational approximation of generalized Mittag-Leffler functions and their inverses: applications to fractional calculus,” *Journal of Computational and Applied Mathematics*, vol. 330, pp. 307–317, 2018.
- [13] A. P. Starovoitov and N. A. Starovoitova, “Padé approximants of the Mittag-Leffler functions,” *Sbornik Mathematics*, vol. 198, no. 7, pp. 1011–1023, 2007.
- [14] A. Borhanifar and S. Valizadeh, “Mittag-Leffler-Padé approximations for the numerical solution of space and time fractional diffusion equations,” *International Journal of Applied Mathematics Research*, vol. 4, no. 4, p. 466, 2015.
- [15] S. Winitzki, “Uniform approximations for transcendental functions,” in *Computational Science and Its Applications — ICCSA 2003*, V. Kumar, M. L. Gavrilova, C. J. K. Tan, and P. L’Ecuyer, Eds. Berlin, Heidelberg: Springer, 2003, pp. 780–789.
- [16] C. Atkinson and A. Osseiran, “Rational solutions for the time-fractional diffusion equation,” *SIAM Journal on Applied Mathematics*, vol. 71, no. 1, pp. 92–106, 2011.
- [17] C. Zeng and Y. Q. Chen, “Global Padé approximations of the generalized Mittag-Leffler function and its inverse,” *Fractional Calculus and Applied Analysis*, vol. 18, no. 6, pp. 1492–1506, 2015.

- [18] C. Ingo, T. R. Barrick, A. G. Webb, and I. Ronen, “Accurate Padé global approximations for the Mittag-Leffler function, its inverse, and its partial derivatives to efficiently compute convergent power series,” *International Journal of Applied and Computational Mathematics*, vol. 3, no. 2, pp. 347–362, 2017.
- [19] J. W. Hanneken, D. M. Vaught, and B. Achar, “Enumeration of the real zeros of the Mittag-Leffler function  $E_\alpha(z)$ ,  $1 < \alpha < 2$ ,” in *Advances in Fractional Calculus*. Springer, 2007, pp. 15–26.
- [20] J. W. Hanneken, B. Achar, and D. M. Vaught, “An alpha-beta phase diagram representation of the zeros and properties of the Mittag-Leffler function,” *Advances in Mathematical Physics*, vol. 2013, 2013.
- [21] J.-S. Duan, Z. Wang, and S.-Z. Fu, “The zeros of the solutions of the fractional oscillation equation,” *Fractional Calculus and Applied Analysis*, vol. 17, no. 1, pp. 10–22, 2014.
- [22] R. Garrappa and M. Popolizio, “Computing the matrix Mittag-Leffler function with applications to fractional calculus,” *Journal of Scientific Computing*, vol. 77, no. 1, pp. 129–153, 2018.
- [23] A. H. Honain and K. M. Furati, “Rational approximation for oscillatory mittag-leffler function,” in *2023 International Conference on Fractional Differentiation and Its Applications (ICFDA)*. IEEE, 2023, pp. 1–5.
- [24] H. J. Haubold, A. M. Mathai, and R. K. Saxena, “Mittag-Leffler functions and their applications,” *Journal of applied mathematics*, vol. 2011, 2011.
- [25] A. Sadeghi and J. R. Cardoso, “Some notes on properties of the matrix Mittag-Leffler function,” *Applied Mathematics and Computation*, vol. 338, pp. 733–738, 2018.
- [26] N. J. Higham, *Functions of matrices: theory and computation*. SIAM, 2008.
- [27] J. G. Aguilar, J. R. Hernández, R. E. Jiménez, C. Astorga-Zaragoza, V. O. Peregrino, and T. C. Fraga, “Fractional electromagnetic waves in plasma,” *Proc. Romanian Acad. A*, vol. 17, no. 1, pp. 31–38, 2014.
- [28] J. Q. Murillo and S. B. Yuste, “An explicit difference method for solving fractional diffusion and diffusion-wave equations in the Caputo form,” *Journal of Computational and Nonlinear Dynamics*, vol. 6, no. 2, 2011.